
Markovian Circuit Tracing for Transformer State Dynamics

Abdullah X

Project AWARE and Zephara AI

founder@zephara.ai; abd.kul956@gmail.com

Abstract

Many sequence computations are easier to study as movement through internal states than as isolated local circuits. We introduce Markovian Circuit Tracing (MCT), a diagnostic pipeline for testing whether transformer activations contain coarse state-transition structure. The benchmark uses synthetic Hidden Markov Model (HMM) tasks where latent states, transition matrices, Bayesian belief vectors, Bayes-optimal predictions, and forced-state counterfactual targets are known exactly. Across six HMM families and three seeds per family, tiny causal transformers learn near-Bayes next-token predictors, with mean excess loss over Bayes of 0.0138. Residual activations contain partial Bayesian belief information in this controlled synthetic benchmark. State abstractions extracted from these activations recover coarse transition signal, strongest in persistent and lower-state regimes, and weaker in ambiguous-emission and six-state regimes. The clearest result comes from state forcing. Patching a recovered-state centroid reduces KL to the exact HMM counterfactual target from 0.1957 in the unpatched model to 0.0532 on average, beating wrong-state, mean-activation, random-activation, and shuffled-label controls. The contribution is a controlled benchmark and evaluation framework for transformer state-dynamics interpretability, with MCT as a simple reference pipeline.

1 Introduction

Mechanistic interpretability studies how trained neural networks compute. Much recent work studies circuits, features, attention heads, activation patching, and causal interventions in transformers (Olah et al., 2020; Elhage et al., 2021; Meng et al., 2022; Conmy et al., 2023). This has produced useful explanations for local behaviors. A different kind of computation appears in partially observed sequence tasks. The model must update an internal summary over time, and that summary must carry information for future prediction.

Hidden Markov Models provide a clean setting for this question. An HMM has an unobserved state sequence, a transition law, and visible emissions. A model trained on visible tokens should learn a predictive summary of the hidden process. In the exact Bayesian solution, that summary is a belief vector over latent states. This makes HMMs useful for interpretability. The experimenter knows the latent states, the belief vectors, the transition matrix, and the exact counterfactual output for forced latent states.

We use this setting to test transformer state dynamics. Markovian Circuit Tracing maps activations to candidate internal states, estimates transitions over those states, tests Markov order, and performs state-forcing interventions. The goal is diagnostic. MCT asks whether a chosen activation-derived state abstraction carries usable transition information. It does not require the model to copy the sampled HMM state. In a partially observed task, a predictive belief-state abstraction can be the more natural target.

This paper contributes a controlled transformer benchmark where automata extraction, predictive-state ideas, probing, activation patching, and causal abstraction can be tested together against exact ground truth. Prior work has studied these components separately. Here the benchmark gives exact latent labels, exact Bayesian beliefs, exact transition matrices, exact Bayes-optimal predictions, and exact forced-state counterfactual targets in one setting (Baum & Petrie, 1966; Rabiner, 1989; Littman et al., 2001; Geiger et al., 2021; Chan et al., 2022).

Markovian Circuit Tracing Architecture

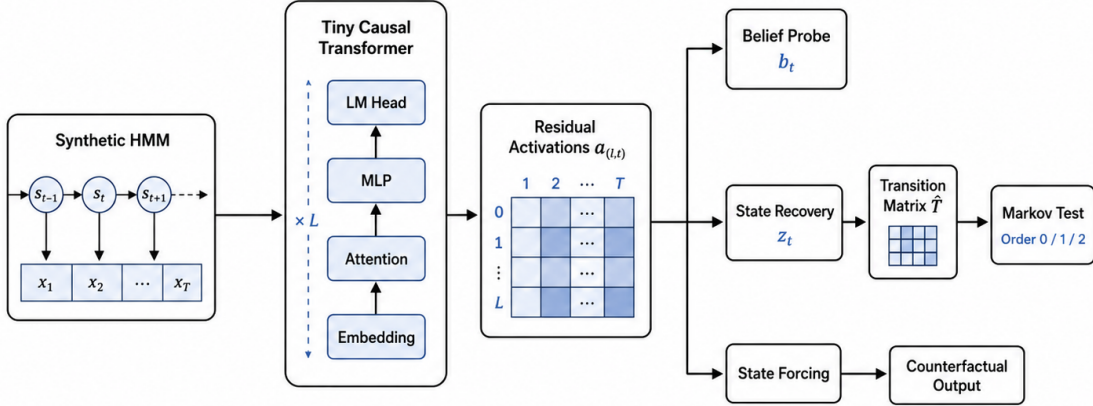


Figure 1: Markovian Circuit Tracing pipeline. A transformer is trained on visible HMM emissions. Activations are used for belief probing, state recovery, transition estimation, Markov-order testing, and counterfactual state forcing.

The empirical result is partial but consistent. Transformers learn the prediction tasks well. Belief information is recoverable from activations in all HMM families, with large family variation. Residual and PCA-based state abstractions recover part of the transition structure, while exact belief clustering remains a stronger upper bound. State forcing gives the clearest evidence that recovered states are causally meaningful in this benchmark. The results support MCT as a benchmarked diagnostic for coarse predictive state dynamics, not as a full hidden-state recovery algorithm.

2 Background and related work

Markov chains and HMMs. A finite Markov chain has states $s_t \in \{1, \dots, K\}$ and transition matrix T with

$$P(s_{t+1} = j \mid s_t = i) = T_{ij}. \quad (1)$$

An HMM adds visible emissions $x_t \in \{1, \dots, V\}$ with emission matrix E , where $E_{iv} = P(x_t = v \mid s_t = i)$. The model observes $x_{1:t}$ but not s_t .

The exact Bayesian belief state is

$$b_t(i) = P(s_t = i \mid x_{1:t}). \quad (2)$$

With row-vector notation, the next-token distribution is

$$P(x_{t+1} \mid x_{1:t}) = b_t T E. \quad (3)$$

This equation is central. A trained transformer may represent a predictive belief state rather than the sampled latent label.

Circuit analysis and interventions. Circuit work analyzes internal mechanisms through components, pathways, and interventions (Olah et al., 2020; Elhage et al., 2021; Conmy et al., 2023). Activation patching and causal tracing test whether chosen activations causally affect model outputs (Meng et al., 2022). Causal scrubbing frames interpretability claims as hypotheses that should pass intervention tests (Chan et al., 2022). MCT uses the same intervention logic, but the HMM benchmark gives exact targets for the intervention.

Probing and state extraction. Linear probes test whether representations contain recoverable information (Alain & Bengio, 2016; Hewitt & Liang, 2019; Belinkov, 2022). Probes alone do not show causal use. Older work extracted finite-state structure from recurrent networks and automata-like models (Cleeremans et al., 1989; Omlin & Giles, 1996; Weiss et al., 2018). Predictive state representations define state by future predictive content rather than by hidden labels (Jaeger, 2000; Littman et al., 2001; Boots et al., 2011). Our benchmark connects these lines of work to transformer activations under exact HMM ground truth.

Sparse features and causal abstraction. Sparse autoencoders and dictionary learning methods study interpretable feature bases in neural activations (Elhage et al., 2022; Cunningham et al., 2023; Bricken et al., 2023). Causal abstraction asks when neural computation supports a higher-level causal model (Geiger et al., 2021). The present paper uses simple residual clustering as a reference extractor. The benchmark is meant to support future extractors, including sparse and probabilistic methods.

3 Markovian Circuit Tracing

Given an activation vector $a_{\ell,t}$ at layer ℓ and time t , MCT applies a state extractor

$$z_t = g(a_{\ell,t}) \in \{1, \dots, M\}. \quad (4)$$

The reference extractor is K-means over residual activations. The recovered transition matrix is

$$\hat{T}_{mn}^{(z)} = \frac{\sum_t \mathbf{1}\{z_t = m, z_{t+1} = n\}}{\sum_t \mathbf{1}\{z_t = m\}}. \quad (5)$$

When $M = K$, we align recovered clusters to true states only for evaluation. This Hungarian matching step is an oracle evaluation step. It is not used in a real unlabeled setting.

MCT evaluates a recovered state sequence through four tests.

1. **Belief recovery.** A linear ridge probe maps $a_{\ell,t}$ to the exact Bayesian belief vector b_t .
2. **Transition recovery.** The aligned $\hat{T}^{(z)}$ is compared with T using row-wise KL and Frobenius error when $M = K$.
3. **Markov order.** Empirical order-0, order-1, and order-2 models over z_t are evaluated by held-out negative log-likelihood.
4. **State forcing.** Recovered-state centroids are patched into the model and compared with exact HMM counterfactual targets.

For a forced latent state i , the next-token target is

$$P(x_{t+1} \mid do(s_t = i)) = e_i T E, \quad (6)$$

where e_i is the one-hot row vector for state i .

The intervention test uses several controls. We compare the unpatched model, the recovered centroid, a wrong recovered centroid, the mean activation, a random activation, a shuffled-label centroid, and a true-state centroid. Lower KL to $e_i T E$ means the patch moves the model closer to the exact counterfactual target.

Table 1: HMM family definitions. K is the hidden-state count and V is the visible-symbol count. $H(T)$ and $H(E)$ are mean transition and emission entropies over the three seeds.

Family	K	V	Transition rule	Emission rule	$H(T)$	$H(E)$	Random per seed
Easy separable	4	6	Banded, $\rho = 0.60$	Dirichlet, $c = 0.20$	0.950 ± 0.000	0.893 ± 0.136	π and emissions
Ambiguous emissions	4	6	Banded, $\rho = 0.60$	Dirichlet, $c = 2.50$	0.950 ± 0.000	1.623 ± 0.053	π and emissions
Persistent	4	6	Sticky, $\rho = 0.82$, fixed small noise	Dirichlet, $c = 0.80$	0.719 ± 0.000	1.263 ± 0.035	π and emissions; fixed T noise
High entropy	4	6	Near-uniform, seed-random	Dirichlet, $c = 1.20$	1.386 ± 0.000	1.395 ± 0.036	π and emissions
Three-state	3	5	Banded, $\rho = 0.64$	Dirichlet, $c = 0.80$	0.903 ± 0.000	1.071 ± 0.098	π and emissions
Six-state	6	8	Banded, $\rho = 0.56$	Dirichlet, $c = 1.00$	0.991 ± 0.000	1.626 ± 0.023	π and emissions

Table 2: Family-level summary. Lower values are better for excess loss, belief KL, and row-wise KL. A larger $0 \rightarrow 1$ NLL gain indicates stronger first-order transition signal.

Family	Excess over Bayes	Belief KL	Cluster acc.	Rowwise KL	NLL gain $0 \rightarrow 1$	NLL gain $1 \rightarrow 2$
Easy	0.027 ± 0.011	0.772 ± 0.109	0.414 ± 0.053	0.265 ± 0.039	0.056 ± 0.033	0.016 ± 0.012
Ambiguous	0.003 ± 0.002	0.152 ± 0.070	0.315 ± 0.018	0.441 ± 0.026	0.004 ± 0.004	0.001 ± 0.002
Persistent	0.029 ± 0.003	0.448 ± 0.015	0.498 ± 0.043	0.388 ± 0.034	0.075 ± 0.021	0.022 ± 0.004
High-entropy	0.001 ± 0.000	0.335 ± 0.041	0.257 ± 0.002	0.027 ± 0.013	0.000 ± 0.000	-0.000 ± 0.001
3-state	0.005 ± 0.001	0.402 ± 0.093	0.484 ± 0.046	0.107 ± 0.034	0.030 ± 0.012	0.004 ± 0.002
6-state	0.017 ± 0.002	0.498 ± 0.032	0.275 ± 0.022	0.673 ± 0.045	0.019 ± 0.005	0.006 ± 0.003

4 Benchmark design

The benchmark uses six HMM families. Table 1 gives the compact definition. Full generation rules are in Appendix A. Each family is run with three seeds. Each model is a two-layer causal transformer with width 128, four attention heads, MLP width 256, and about 275k parameters. Runs use sequences of length 64, 6000 training sequences, and 1500 validation sequences.

The benchmark evaluates residual K-means, PCA plus K-means, random-projection plus K-means, exact belief K-means, token baselines, and a true-state oracle. It also sweeps cluster counts $M \in \{2, 3, 4, 5, 6, 8, 10\}$ and layers from embeddings through the final layer-normalized stream. The main text reports the main results. Appendix C gives the full protocol and additional tables.

5 Results

5.1 Task learning and transition signal vary by HMM family

Across all eighteen runs, the mean validation loss is 1.7044 and the mean Bayes-optimal loss is 1.6907. The mean excess loss over Bayes is 0.0138. The models therefore learn the prediction task well. Table 2 shows the main metrics by family.

The strongest first-order signal appears in the persistent and easy-separable families. The ambiguous-emission and high-entropy families show weak order gains. The six-state family is harder for transition recovery. This variation is useful because it shows that the benchmark is not solved by a single trivial pattern.

5.2 Activation-derived states recover part of the belief-state structure

Figure 3 compares true- K transition recovery. Belief K-means is the strongest non-oracle target in most families. Residual K-means and PCA plus K-means recover part of the structure. Random-projection K-means is weaker. This shows that the benchmark has headroom. The current reference extractor does not saturate the task.

The gap to belief clustering is important. It means the model’s predictive state is better viewed as a belief-like object than as a direct copy of the sampled HMM label. The residual extractor turns that continuous structure into a coarse discrete state. This explains why recovered transition matrices are smoothed.

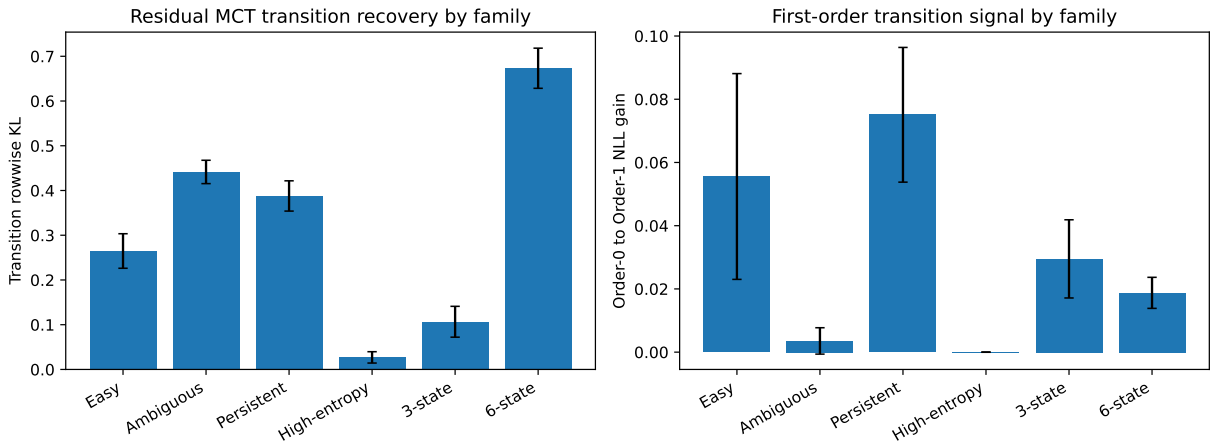


Figure 2: Family-level behavior. Left, residual MCT transition row-wise KL. Right, held-out order-0 to order-1 NLL gain. Persistent and easy-separable families show stronger first-order signal. High entropy acts as a weak-signal control.

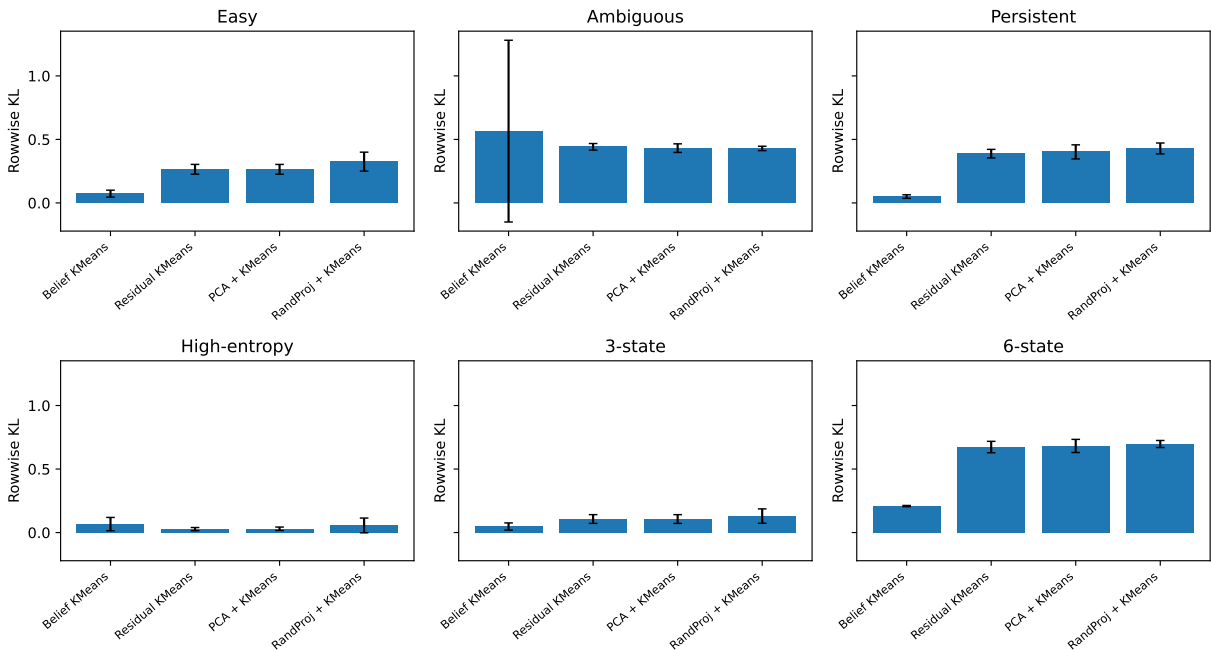


Figure 3: True- K transition comparison by HMM family. Exact belief clustering is a strong upper bound. Residual and PCA-based activation abstractions recover part of the transition structure.

5.3 Layer and cluster-count sweeps support the diagnostic use of MCT

Layer sweeps show that state structure often becomes clearer deeper in the model. Figure 4 reports row-wise transition KL and belief-probe KL across layers. The pattern is strongest for the easy-separable and persistent families. The high-entropy family stays weak across layers, as expected from its near-uniform transition law.

Cluster-count sweeps remain useful when $M \neq K$. Direct matrix comparison is then inappropriate, so we use belief reconstruction KL and next true-state NLL. These results are reported in Appendix C. The main finding is stable. MCT behaves as a coarse predictive-state diagnostic, not as an exact state-label recovery tool.

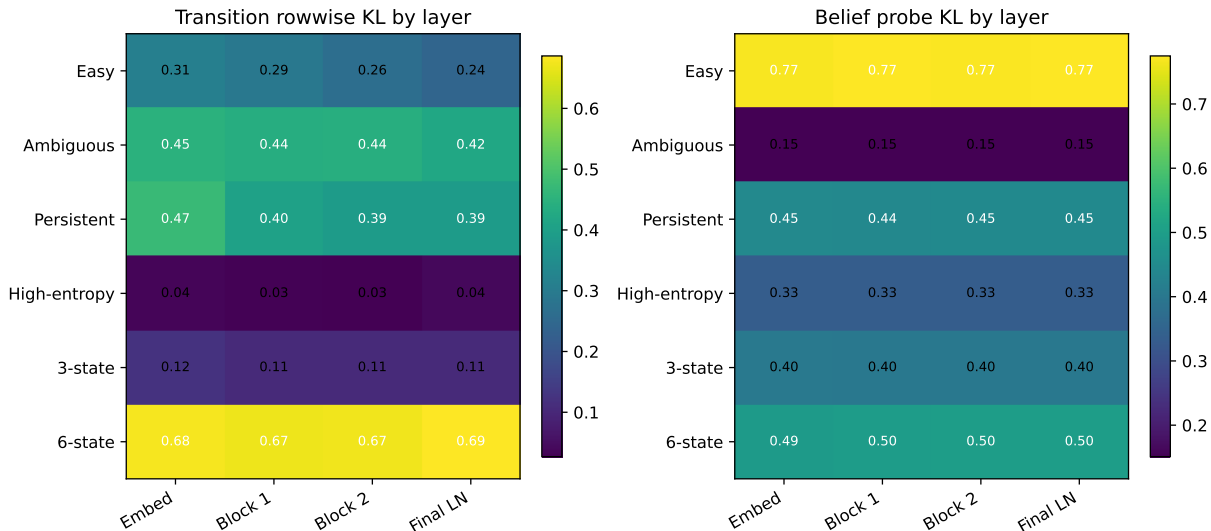


Figure 4: Layer-wise results. Later layers often expose stronger transition and belief structure, though the pattern depends on the HMM family.

Table 3: State-forcing controls aggregated across all families, seeds, and target states. Lower KL is better.

Patch type	KL to target	Improvement over unpatched
Unpatched	0.196 ± 0.186	0.000 ± 0.000
Recovered centroid	0.053 ± 0.064	0.143 ± 0.150
True-state centroid	0.074 ± 0.062	0.122 ± 0.135
Mean activation	0.147 ± 0.162	0.049 ± 0.065
Random activation	0.167 ± 0.170	0.029 ± 0.076
Shuffled-label centroid	0.157 ± 0.213	0.039 ± 0.193
Wrong-state centroid	0.206 ± 0.219	-0.010 ± 0.110

5.4 State forcing gives the strongest evidence

Table 3 and Figure 5 show the intervention result. The unpatched model has mean KL 0.1957 to the exact forced-state target. The recovered-centroid patch reduces this to 0.0532. The improvement over the unpatched model is 0.1425. It beats wrong-state, mean-activation, random-activation, shuffled-label, and true-state centroid controls on average.

This result supports causal use of the recovered state abstraction in this controlled benchmark. It also explains why true hidden labels are not always the best intervention grouping. The model’s useful internal state can be closer to a predictive or belief-state abstraction than to the sampled latent state label.

6 Discussion and limitations

MCT is best read as a benchmarked diagnostic for transformer state dynamics. The results show partial recovery of coarse transition structure in small synthetic HMM tasks. They also show clear limits. Belief clustering remains a stronger upper bound, token baselines can be strong in some families, and six-state or ambiguous-emission regimes are harder. These findings make the benchmark useful because it exposes where a method works and where it fails.

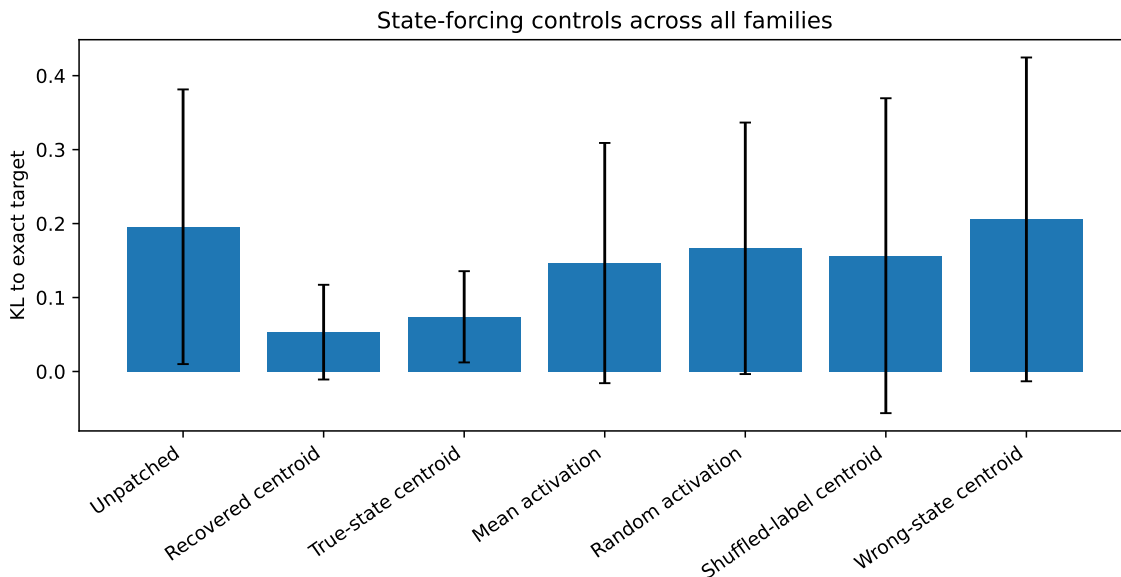


Figure 5: State-forcing controls. Recovered-centroid patching gives the lowest KL to the exact HMM counterfactual target among the tested conditions.

The work has several limits. The tasks are synthetic, the models are tiny, and the reference extractor is simple. The benchmark does not show full causal abstraction between a transformer and an HMM. It also does not show that natural-language reasoning has the same state structure. The claim is narrower. In controlled HMM families, activation-derived state abstractions can expose coarse predictive transition dynamics, and state-forcing tests can evaluate their causal relevance against exact targets.

Future work should test learned state extractors, probabilistic state models over activations, continuous belief-state comparisons, and richer partially observed environments. The benchmark can also be paired with feature-level analysis to identify which model components implement the observed state updates.

7 Conclusion

This paper introduced Markovian Circuit Tracing for transformer state dynamics and evaluated it on a controlled HMM benchmark. The benchmark gives exact beliefs, transitions, Bayes-optimal predictions, and forced-state targets. The results support MCT as a clear diagnostic framework. It detects partial predictive transition structure, shows where the signal is weak, and provides strong intervention controls through exact HMM counterfactuals.

References

- Guillaume Alain and Yoshua Bengio. Understanding intermediate layers using linear classifier probes. *arXiv preprint arXiv:1610.01644*, 2016.
- Leonard E. Baum and Ted Petrie. Statistical inference for probabilistic functions of finite state Markov chains. *The Annals of Mathematical Statistics*, 37(6):1554–1563, 1966.
- Yonatan Belinkov. Probing classifiers: Promises, shortcomings, and advances. *Computational Linguistics*, 48(1):207–219, 2022.
- Byron Boots, Sajid Siddiqi, and Geoffrey J. Gordon. Closing the learning-planning loop with predictive state representations. *The International Journal of Robotics Research*, 30(7):954–966, 2011.

-
- Trenton Bricken, Adly Templeton, Joshua Batson, Brian Chen, Adam Jermyn, Shan Carter, and Chris Olah. Towards monosemanticity: Decomposing language models with dictionary learning, 2023. arXiv:2310.01881.
- Lawrence Chan, Adria Garriga-Alonso, Nicholas Goldowsky-Dill, Ryan Greenblatt, Elena Nitishinskaya, Ansh Radhakrishnan, and Buck Shlegeris. Causal scrubbing: A method for rigorously testing interpretability hypotheses, 2022. arXiv:2212.06861.
- Axel Cleeremans, David Servan-Schreiber, and James L. McClelland. Finite state automata and simple recurrent networks. *Neural Computation*, 1(3):372–381, 1989.
- Arthur Conmy, Augustine Mavor-Parker, Aengus Lynch, Stefan Heimersheim, and Adria Garriga-Alonso. Towards automated circuit discovery for mechanistic interpretability. In *Advances in Neural Information Processing Systems*, 2023.
- Hoagy Cunningham, Aidan Ewart, Logan Riggs, Robert Huben, and Lee Sharkey. Sparse autoencoders find highly interpretable features in language models, 2023. arXiv:2309.08600.
- Nelson Elhage, Neel Nanda, Catherine Olsson, Tom Henighan, Nicholas Joseph, Ben Mann, Amanda Askell, Yuntao Bai, Anna Chen, Tom Conerly, et al. A mathematical framework for transformer circuits, 2021. Transformer Circuits Thread.
- Nelson Elhage, Tristan Hume, Catherine Olsson, Nicholas Schiefer, Tom Henighan, Shauna Kravec, Zac Hatfield-Dodds, Robert Lasenby, Dawn Drain, Carol Chen, et al. Toy models of superposition, 2022. Transformer Circuits Thread.
- Atticus Geiger, Hanson Lu, Thomas Icard, and Christopher Potts. Causal abstractions of neural networks. In *Advances in Neural Information Processing Systems*, 2021.
- John Hewitt and Percy Liang. Designing and interpreting probes with control tasks. In *Proceedings of the 2019 Conference on Empirical Methods in Natural Language Processing*, pages 2733–2743, 2019.
- Herbert Jaeger. Observable operator models for discrete stochastic time series. *Neural Computation*, 12(6):1371–1398, 2000.
- Michael L. Littman, Richard S. Sutton, and Satinder Singh. Predictive representations of state. In *Advances in Neural Information Processing Systems*, 2001.
- Kevin Meng, David Bau, Alex Andonian, and Yonatan Belinkov. Locating and editing factual associations in GPT. In *Advances in Neural Information Processing Systems*, 35:17359–17372, 2022.
- Joshua Michalenko, Ameesh Shah, Abhinav Verma, Richard Baraniuk, Suraj Chaudhuri, and Ankit B. Patel. Interpreting recurrent neural networks behavior via excitable network attractors. In *ICML Workshop on Understanding and Improving Generalization in Deep Learning*, 2019.
- Michael C. Mozer. A focus on recurrent networks. In *Connectionist Models Summer School*, 1989.
- Neel Nanda, Lawrence Chan, Tom Lieberum, Jess Smith, and Jacob Steinhardt. Progress measures for grokking via mechanistic interpretability, 2023. arXiv:2301.05217.
- Chris Olah, Nick Cammarata, Ludwig Schubert, Gabriel Goh, Michael Petrov, and Shan Carter. Zoom in: An introduction to circuits. *Distill*, 5(3), 2020.
- Christian W. Omlin and C. Lee Giles. Extraction of rules from discrete-time recurrent neural networks. *Neural Networks*, 9(1):41–52, 1996.
- Lawrence R. Rabiner. A tutorial on hidden Markov models and selected applications in speech recognition. *Proceedings of the IEEE*, 77(2):257–286, 1989.
- Gail Weiss, Yoav Goldberg, and Eran Yahav. Practical finite state automata extraction from recurrent neural networks. In *International Conference on Learning Representations*, 2018.

A HMM family definitions

Each family is generated from the same code path. The initial distribution π is sampled from a symmetric Dirichlet distribution over the hidden states for each seed. Sequences have length 64. Each full benchmark run uses 6000 training sequences and 1500 validation sequences. The validation split is used for reporting activations and metrics. The experiments are synthetic, and there is no external dataset.

For banded transition families, each state has self-transition probability ρ . The remaining probability mass is split across the previous and next state in a circular banded structure. For sticky families, the diagonal receives probability ρ and the remaining probability mass is spread across other states, with a small fixed noise term before row normalization. For the high-entropy family, transition rows are near-uniform with a small seed-random perturbation before row normalization.

Emission distributions are sampled from Dirichlet rows. Each row receives a base concentration c , with extra mass placed on state-associated visible symbols before sampling. Lower c gives more separable emissions. Higher c gives more ambiguous emissions. The compact family table is repeated below.

Table 4: HMM family generation rules. Transition and emission entropies are mean \pm standard deviation over the three seeds.

Family	K	V	Transition rule	Emission rule	$H(T)$	$H(E)$	Random per seed
Easy separable	4	6	Banded, $\rho = 0.60$	Dirichlet, $c = 0.20$	0.950 ± 0.000	0.893 ± 0.136	π and emissions
Ambiguous emissions	4	6	Banded, $\rho = 0.60$	Dirichlet, $c = 2.50$	0.950 ± 0.000	1.623 ± 0.053	π and emissions
Persistent	4	6	Sticky, $\rho = 0.82$, fixed small noise	Dirichlet, $c = 0.80$	0.719 ± 0.000	1.263 ± 0.035	π and emissions; fixed T noise
High entropy	4	6	Near-uniform, seed-random	Dirichlet, $c = 1.20$	1.386 ± 0.000	1.395 ± 0.036	π and emissions
Three-state	3	5	Banded, $\rho = 0.64$	Dirichlet, $c = 0.80$	0.903 ± 0.000	1.071 ± 0.098	π and emissions
Six-state	6	8	Banded, $\rho = 0.56$	Dirichlet, $c = 1.00$	0.991 ± 0.000	1.626 ± 0.023	π and emissions

B Intervention protocol

The forcing experiment uses the second post-residual layer, denoted `resid_post_1`. The patch position is token position 20, clipped to the sequence length when needed. A fixed subset of validation sequences is used for intervention evaluation. In the full benchmark this subset contains up to 256 validation sequences per family and seed.

Clustering is fit on validation activations in the current implementation. Centroids are also computed from validation activations. This keeps the analysis simple and matched to the reported state sequence. A stricter train-validation-test split would fit clusters and centroids on training activations and evaluate interventions on held-out activations. The current result should be read as a controlled benchmark result, not as a deployment protocol.

Recovered clusters are aligned to target HMM labels with Hungarian matching when the cluster count equals the true number of hidden states. This matching is used only for evaluation and for assigning recovered centroids to target-state interventions. The wrong-state centroid uses the next aligned state in cyclic order. Shuffled-label centroids are built by applying a random permutation to the recovered-state labels before assigning centroids. The mean-activation patch uses the average recovered centroid. The random-activation patch samples a Gaussian vector with mean and standard deviation matched to the recovered centroids. The true-state centroid groups activations by the sampled hidden state labels.

For target state i , the forced-state target is $e_i T E$, where e_i is the one-hot row vector for state i . This target corresponds to forcing the current latent state before one HMM transition and one emission step. KL is computed between the patched model’s next-token distribution at the patched position and this exact target. Results are averaged across sequences, target states, families, and seeds. Family-wise averages are reported in Appendix C.

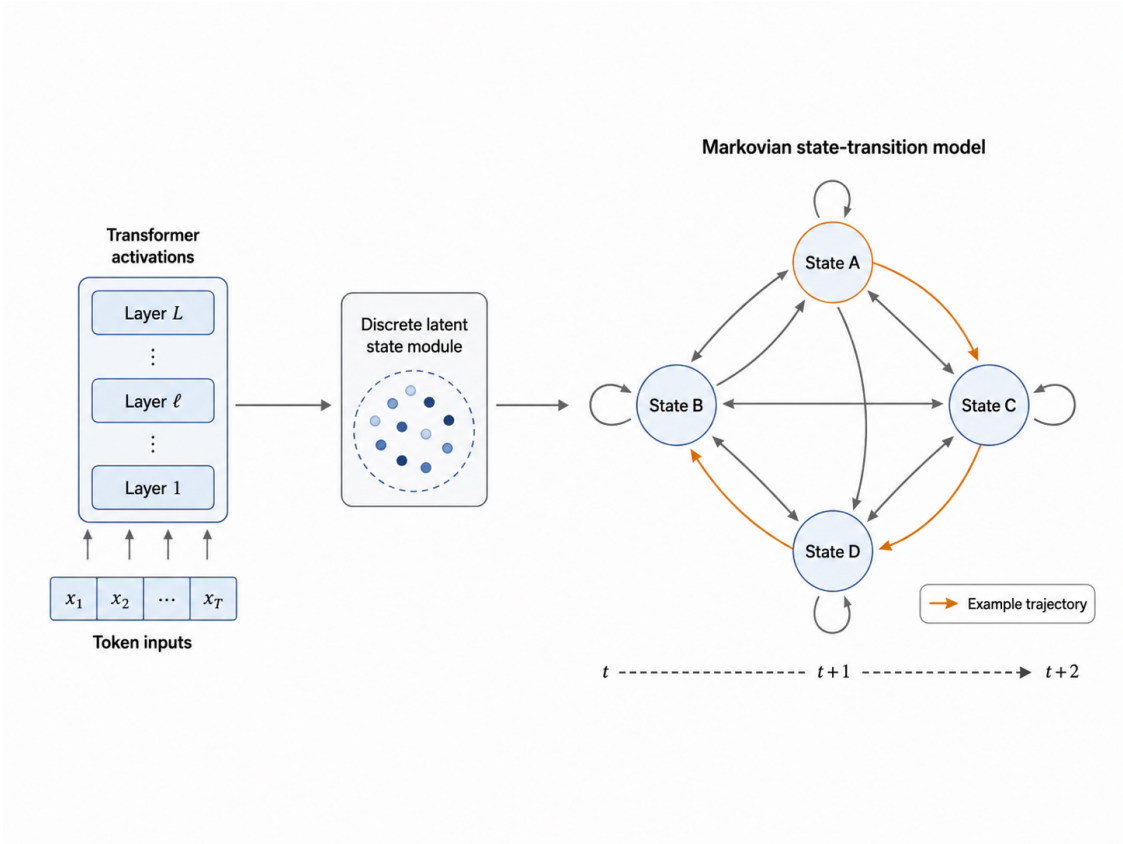


Figure 6: Conceptual Markovian state-transition view used by the benchmark. The diagram is illustrative and does not encode numeric probabilities.

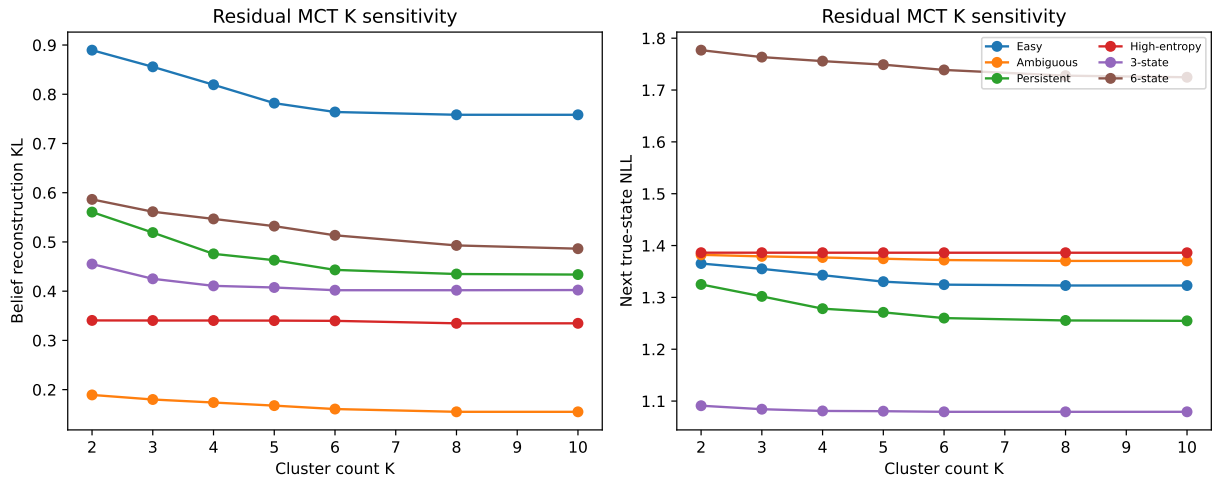


Figure 7: Residual MCT under cluster-count misspecification. Left, belief reconstruction KL. Right, next true-state NLL.

Table 5: True- K baseline comparison. Lower values are better.

Family	Method	K	Rowwise KL	Belief recon. KL	Next true-state NLL
Easy	Belief KMeans	4	0.073 \pm 0.027	0.131 \pm 0.048	1.181 \pm 0.066
Easy	Residual KMeans	4	0.265 \pm 0.039	0.819 \pm 0.091	1.343 \pm 0.019
Easy	PCA + KMeans	4	0.264 \pm 0.039	0.813 \pm 0.096	1.341 \pm 0.019
Easy	RandProj + KMeans	4	0.325 \pm 0.075	0.859 \pm 0.087	1.356 \pm 0.021
Ambiguous	Belief KMeans	4	0.565 \pm 0.715	0.057 \pm 0.032	1.342 \pm 0.024
Ambiguous	Residual KMeans	4	0.441 \pm 0.026	0.174 \pm 0.074	1.377 \pm 0.008
Ambiguous	PCA + KMeans	4	0.431 \pm 0.034	0.176 \pm 0.077	1.378 \pm 0.007
Ambiguous	RandProj + KMeans	4	0.429 \pm 0.017	0.186 \pm 0.088	1.381 \pm 0.002
Persistent	Belief KMeans	4	0.050 \pm 0.014	0.159 \pm 0.014	1.108 \pm 0.020
Persistent	Residual KMeans	4	0.388 \pm 0.034	0.476 \pm 0.031	1.278 \pm 0.021
Persistent	PCA + KMeans	4	0.402 \pm 0.056	0.484 \pm 0.046	1.283 \pm 0.027
Persistent	RandProj + KMeans	4	0.429 \pm 0.043	0.532 \pm 0.040	1.308 \pm 0.020
High-entropy	Belief KMeans	4	0.067 \pm 0.052	0.040 \pm 0.021	1.386 \pm 0.000
High-entropy	Residual KMeans	4	0.027 \pm 0.013	0.340 \pm 0.037	1.386 \pm 0.000
High-entropy	PCA + KMeans	4	0.030 \pm 0.014	0.340 \pm 0.037	1.386 \pm 0.000
High-entropy	RandProj + KMeans	4	0.056 \pm 0.058	0.340 \pm 0.037	1.386 \pm 0.000
3-state	Belief KMeans	3	0.048 \pm 0.028	0.075 \pm 0.009	1.016 \pm 0.026
3-state	Residual KMeans	3	0.107 \pm 0.034	0.425 \pm 0.099	1.084 \pm 0.006
3-state	PCA + KMeans	3	0.107 \pm 0.034	0.425 \pm 0.099	1.084 \pm 0.006
3-state	RandProj + KMeans	3	0.130 \pm 0.057	0.435 \pm 0.109	1.086 \pm 0.005
6-state	Belief KMeans	6	0.208 \pm 0.005	0.194 \pm 0.019	1.619 \pm 0.021
6-state	Residual KMeans	6	0.673 \pm 0.045	0.513 \pm 0.036	1.739 \pm 0.014
6-state	PCA + KMeans	6	0.682 \pm 0.052	0.517 \pm 0.042	1.741 \pm 0.018
6-state	RandProj + KMeans	6	0.697 \pm 0.028	0.545 \pm 0.042	1.755 \pm 0.012

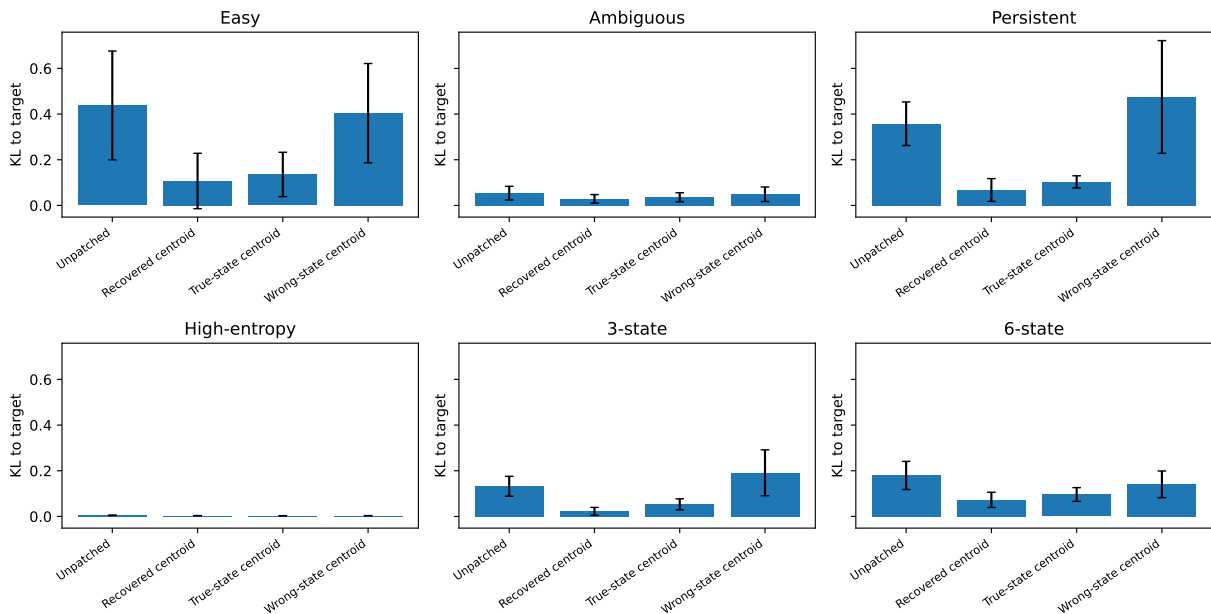


Figure 8: State-forcing controls by family. Recovered-centroid patching is strongest in the families with clearer transition structure.

C Additional results

D Reproducibility note

The supplementary material contains the source files, figures, tables, and benchmark outputs needed to inspect and rebuild the paper package. All tables and plots in the paper are generated from CSV or JSON

Table 6: Layer-wise results for each family. Lower belief KL and row-wise KL are better.

Family	Layer	Belief KL	Cluster acc.	Rowwise KL
Easy	Embed	0.768 \pm 0.106	0.405 \pm 0.030	0.311 \pm 0.025
Easy	Block 1	0.775 \pm 0.110	0.421 \pm 0.051	0.290 \pm 0.057
Easy	Block 2	0.772 \pm 0.109	0.414 \pm 0.053	0.265 \pm 0.039
Easy	Final LN	0.775 \pm 0.108	0.438 \pm 0.071	0.241 \pm 0.069
Ambiguous	Embed	0.153 \pm 0.069	0.318 \pm 0.016	0.448 \pm 0.019
Ambiguous	Block 1	0.152 \pm 0.069	0.323 \pm 0.037	0.439 \pm 0.030
Ambiguous	Block 2	0.152 \pm 0.070	0.315 \pm 0.018	0.441 \pm 0.026
Ambiguous	Final LN	0.151 \pm 0.068	0.323 \pm 0.038	0.419 \pm 0.011
Persistent	Embed	0.445 \pm 0.028	0.424 \pm 0.048	0.473 \pm 0.033
Persistent	Block 1	0.442 \pm 0.008	0.471 \pm 0.086	0.403 \pm 0.055
Persistent	Block 2	0.448 \pm 0.015	0.498 \pm 0.043	0.388 \pm 0.034
Persistent	Final LN	0.447 \pm 0.011	0.500 \pm 0.041	0.389 \pm 0.036
High-entropy	Embed	0.334 \pm 0.041	0.256 \pm 0.003	0.037 \pm 0.011
High-entropy	Block 1	0.335 \pm 0.041	0.256 \pm 0.003	0.030 \pm 0.014
High-entropy	Block 2	0.335 \pm 0.041	0.257 \pm 0.002	0.027 \pm 0.013
High-entropy	Final LN	0.335 \pm 0.041	0.256 \pm 0.003	0.040 \pm 0.035
3-state	Embed	0.402 \pm 0.093	0.481 \pm 0.047	0.122 \pm 0.044
3-state	Block 1	0.402 \pm 0.093	0.484 \pm 0.046	0.107 \pm 0.034
3-state	Block 2	0.402 \pm 0.093	0.484 \pm 0.046	0.107 \pm 0.034
3-state	Final LN	0.402 \pm 0.093	0.488 \pm 0.051	0.105 \pm 0.035
6-state	Embed	0.491 \pm 0.033	0.265 \pm 0.017	0.677 \pm 0.024
6-state	Block 1	0.496 \pm 0.036	0.269 \pm 0.027	0.670 \pm 0.041
6-state	Block 2	0.498 \pm 0.032	0.275 \pm 0.022	0.673 \pm 0.045
6-state	Final LN	0.497 \pm 0.033	0.278 \pm 0.022	0.686 \pm 0.057

Table 7: Family-wise state-forcing results for the main controls. Lower KL is better.

Family	Unpatched	Recovered centroid	True-state centroid	Wrong-state centroid
Easy	0.438 \pm 0.238	0.107 \pm 0.121	0.136 \pm 0.097	0.404 \pm 0.218
Ambiguous	0.054 \pm 0.030	0.029 \pm 0.019	0.036 \pm 0.020	0.049 \pm 0.032
Persistent	0.358 \pm 0.096	0.068 \pm 0.050	0.103 \pm 0.027	0.475 \pm 0.247
High-entropy	0.005 \pm 0.001	0.003 \pm 0.001	0.003 \pm 0.000	0.003 \pm 0.000
3-state	0.132 \pm 0.044	0.022 \pm 0.017	0.053 \pm 0.024	0.191 \pm 0.100
6-state	0.180 \pm 0.062	0.073 \pm 0.033	0.096 \pm 0.030	0.141 \pm 0.058

artifacts produced by the benchmark workflows. The workflow design is part of the benchmark contribution, since each claim depends on exact experimental artifacts rather than manual transcription.